United States Department of Commerce
Technology Administration
National Institute of Standards and Technology

NIST Special Publication 919

International Workshop on Fire Performance of High-Strength Concrete, NIST, Gaithersburg, MD, February 13-14, 1997 Proceedings

Long T. Phan, Nicholas J. Carino, Dat Duthinh, and Edward Garboczi

B.8 Measurement and Prediction of Pore Pressure in Cement Mortar Subjected to Elevated Temperature

Gary R. Consolazio [1]

Michael C. McVay [2]

Jeff W. Rish III [3]

ABSTRACT

When a partially saturated porous medium is subjected to a high temperature heating source, pore pressures large enough to initiate explosive spalling may be developed within the pore spaces of the material. The level to which these pore pressures ultimately rise depends on the saturation and permeability of the medium as well as the rate at which heat flows into the material. In this paper, experimental and numerical studies involving the measurement and prediction of pore pressures and moisture flow in concrete are presented. The results of isothermal flow tests are presented in order to evaluate the accuracy of Darcy's law and the influence of Klinkenberg's effect in gas flows. Pore pressure data are presented for experimental tests in which saturated cement mortar specimens were subjected to high temperature radiant heating conditions. A numerical modeling technique is then presented and is used to numerically simulate the experimental tests. Close agreement is shown between the pore pressures and temperatures recorded experimentally and those predicted through simulation.

INTRODUCTION

Evaluation of airfield pavement degradation and fire safety evaluation of concrete structures are examples of situations that involve moist porous media (e.g. concrete) subjected to severe thermal loadings. The presence of moisture in heated porous media gives rise to internal pore pressures that, in combination with differential thermal stresses, can cause explosive spalling of the material. Spalling of this type can cause rapid degradation of concrete airfield pavements as well as presenting fire safety considerations for concrete structures subjected to fires. In addition, some experimental studies (Sanjayan and Stocks 1993) have suggested that, due to its lower permeability, high-strength concrete may be more prone to explosive spalling than normal-strength concrete.

Internal pore pressure buildup for porous media subjected to thermal loading is more severe for materials that have lower permeability. However, there is conflicting experimental data on this issue (Jahren 1989). Therefore, gaining an understanding of moist porous media subjected to fires and formulating a model to predict its behavior under such circumstances is highly desirable.

[1] Assistant Professor, Rutgers University, Dept. of Civil & Environmental Engineering, P.O. Box 909, Piscataway, NJ, 08855 (grc@civeng.rutgers.edu).

[2] Professor, University of Florida, Dept. of Civil Engineering, 345 Weil Hall, Gainesville, FL, 32611 (mcm@ce.ufl.edu).

[3] Research Engineer, WL/FIVCO, Tyndall AFB, FL 32403. Currently Mechanical Engineer, Coastal Systems Station, Dahlgren Division, Panama City, FL 32407.

ISOTHERMAL FLOW STUDY

The primary impetus for the work presented herein originated from problems involving spalling of concrete airfield surfaces. Concrete surfaces located where they are subjected to streams of hot jet exhaust often sustain significant surface spalling. To study the influence of pore pressure on spalling, the United States Air Force initiated steady state and transient testing of cement mortar.

To model both the mass and heat migration through cement, coupled partial differential equations concerning the conservation of mass, momentum and energy must be solved. In the case of the momentum of the fluid, Darcy's (1856) expression is used, whereas for gas, Darcy or Klinkenberg's (1941) equation is employed. The former is linear with pressure gradient and the latter is nonlinear.

In this portion of the work, the primary concern was quantifying the error of Darcy's expression over Klinkenberg's equation for gas flow in cement under elevated temperatures. The effort involved eighteen isothermal steady state flow tests with pressures varying from 5 to 20 atmospheres for which flow and pressure across the specimens were monitored. Both superheated steam and nitrogen gas were employed.

For the isothermal transient tests, both nitrogen and superheated steam were passed through specimens while monitoring flow rates. Results of the testing (McVay and Rish 1995) revealed that the flow of gases and vapors at the pressures expected (1350-3500 kPa) resulted in slip flow, not laminar flow, thus requiring a modification to Darcy's law. Using Klinkenberg's modification, a theoretical expression for pressure under stead-state conditions was developed that compares favorably to experimental data. It was found that Klinkenberg's expression was capable of predicting all the flow and pressure results within a few percent, whereas Darcy's expression was in error by 15% to 25% for both pressure and flow results.

MOISTURE CLOG SPALLING

Spalling of moist concrete and other moist porous materials subjected to high temperature heat sources can be attributed primarily to two mechanisms—thermal gradients and pore pressures. Steep thermal gradients in a solid material—whether a porous solid or not—can cause significant differential thermal stresses to be developed. If these thermal stresses are sufficiently large, spalling may occur. In moist porous materials, i.e. porous materials that are at least partially saturated, build up of pore pressures during heating can also have a very substantial influence on the likelihood of spalling. As liquid pore water vaporizes and migrates through the porous solid skeleton of the material, pore pressures can become large enough to cause spalling. In most cases of heat induced spalling, a combination of these two mechanisms is in effect.

Moisture clog spalling (Hamarthy 1965, Smith 1978) is the name given to the process by which large pore pressures can be produced when a moist porous medium is heated. The presence of entrapped moisture in a porous media exposed to high temperature can be either beneficial or detrimental, with one of the primary deciding factors being the rate of heating, the permeability of the material, and the moisture level. Porous materials such as concrete and cement mortar contain free liquid water, adsorbed (bound) water, vaporized water, and air in their pore spaces. The quantity of such pore water is a function of many factors including the initial water/cement (w/c) ratio at time of casting, the age of the material, and environmental conditions. The rate of heating will be a function of the temperature of the heat source and the nature of the heat transfer (i.e., conduction, convection, radiation) from the source to the porous medium.

During severe thermal loading, heat flow into the material will result in an increase in the temperature of the solid skeleton and the pore water. When the pore water reaches a high enough temperature—which is dependent on, among other things, the pore pressure—it will begin to vaporize. A portion of the heat flow into the material will be consumed by this pore water vaporization process (Šelih et al. 1994). As such, the presence of pore water is beneficial because it slows the rate at which the temperature of the solid skeleton rises. However, when the pore water vaporizes, an increase in pore pressure will result. As the pore pressures increases, a pressure gradient will form between the zone of vaporization and lower pressure regions deeper inside the concrete and at the exterior surface of the material. This is illustrated through numerical simulation later in this paper. Also, as the pore water temperature increases, thermal expansion of the liquid phase will occur (Kodres 1996) which can also increase the pore pressure. As the vapor migrates along the pressure gradient, it will either escape to the atmosphere, or move inward in the material reaching a lower temperature region and condensing. Such vapor migration will relieve the buildup of pore pressure at the zone of vaporization but will also increase the saturation level.

The portion of the vapor that migrates deeper into the concrete will condense because the temperature in this region will generally be cooler than that at the vaporization region. As the migrated vapor condenses, it will add to the liquid pore water already present in the pore spaces of the cooler region. As the vaporize-migrate-condense cycle continues, accumulation of pore water will build up in the cooler regions until finally a completely saturated layer is formed. Once this layer forms, vaporized pore water is severely impeded from migrating inward in the concrete due to the saturated front. Instead it is forced to migrate through the dry region to escape into the atmosphere. If the permeability of the material is sufficiently low or the rate of heating sufficiently high, vaporized water will not be able to escape fast enough to keep internal pore pressures from rising inside the material. Spalling will occur when the tensile strength of the concrete is exceeded by the combination of pore pressure and thermal stresses. The complete process is illustrated in Figure 1.

The "moisture clog spalling" concept presented above has been substantiated in various forms by other researchers (Sahota and Pagni 1979, Kodres 1996). A fundamental aspect of this scenario is that the rate of heating, the saturation level, and the permeability of the material can determine whether or not spalling occurs. If the rate of heating or the saturation level are sufficiently low or the material permeability is sufficiently large, vaporized pore water will be able to escape under a smaller pressure gradient. Alternatively, if rate of heating and the saturation level are high or the concrete permeability is small, then the rate at which vapor is produced at the saturated front can exceed the rate at which it escapes to the atmosphere and very large pore pressures can result.

EXPERIMENTAL PROGRAM

The experimental program consisted of subjecting two nearly saturated cement mortar specimens to a high temperature radiant heating source and measuring the transient pore pressures and temperatures from the resulting thermally driven flow. To obtain repeatable results, as well as to remove the influence of aggregate type and size, the tests were performed on cement mortar as opposed to concrete. Two mortar specimens were cast in steel circular molds and consolidated through vibration. They were then allowed to hydrate (cure) for two days in the molds after which they were placed in a water bath so that they could reach a nearly saturated state. Tests on identically prepared cement mortar samples revealed a porosity (volume of voids to total volume) of 17.5% and a permeability of approximately 8.324E-17 m^2.

The two specimens were instrumented by installing thermocouples and pore pressure transducers in the positions shown in Figure 2. The thermocouples were installed by drilling holes from the bottom of the specimen up to the desired vertical elevation, inserting the thermocouples, and then cementing them into the drilled holes. Since high temperatures and pressures were anticipated for the experiment, special sealed, thermally compensated pore pressure transducers (PPTs) were used to measure pore pressure. The PPTs were installed in such a way that they could be recovered for reuse after the experiment was completed. First, a metal lag bolt was hollowed out by drilling a hole lengthwise through the bolt. A PPT was then epoxied into the hollow portion of the bolt such that the transducer was at the tip of the bolt. A larger diameter hole was then drilled into the mortar specimen and the lag bolt was cemented into the drilled hole.

A portable cylindrical oven of approximately the same diameter as the specimens served as the radiant heat source. The sides of the oven walls consisted of heating elements embedded in ceramic material while the top (cap) of the oven consisted of insulation. A thermocouple was placed inside the oven near the top surface to monitor the transient air temperature in the oven. Just prior to testing, the temperature of the oven was raised to approximately 925C.

Testing consisted of heating the oven to the testing temperature, then lifting it up and placing it adjacent to the top of the specimen. In this manner, each specimen "saw" the heat as being applied in a rapid fashion rather than experiencing a gradual increase in temperature during oven warm-up. Rapid heating is consistent with the type of thermal loading experienced by concrete runways subjected to jet exhaust. Two test runs were performed—one on each cement mortar specimen. In each case, the test was allowed to continue until it was determined that the PPTs would soon experience damage. At that point (around 500 seconds into the tests), the oven was removed from the specimen. In each test, spalling of the mortar surface was observed prior to removal of the oven. Temperature and pore pressures inside the specimens continued to be recorded after the heat source was removed so that the cool down behavior of the material could be observed as well.

Transient temperatures for the two test runs are shown in Figure 3. In each case, the point at which the oven was removed is evident from the shape of the temperature curves for the thermocouples nearest the specimen surface (i.e., at 1.5 mm for test-1 and at 3.5 mm for test-2). A sharp decline in temperature near the surface and a more gradual decline in temperature deeper inside the specimen can be observed after removal of the oven.

One can see from the figure that there is a sharp temperature gradient in each specimen. For example, by looking at the temperatures near the surface (at 1.5 mm and 3.5 mm) and those deeper in the specimens (at 19 mm) one observes that as time increases (up to the oven cutoff time), there is a considerable temperature difference. This temperature difference occurs over only a distance of 17.5 mm for test-1 (19 mm-1.5 mm=17.5 mm) and 15.5 mm for test-2 (19 mm-3.5 mm=15.5 mm).

Pore pressures for the two tests are shown in Figure 4. As was anticipated, significant pressures—on the order of 3100 kPa—were developed in each case. Thus, the concept of pore pressure buildup as a contributor to the initiation of spalling was confirmed experimentally. The unique, and somewhat curious shape of the pore pressure curves, i.e. the double pressure peaks and the dip in between them, is due to a peculiarity of the PPT installation. After the tests were completed, the PPTs were removed and the depth of the drilled shaft measured carefully. By subtracting the known length of the bolt, it was found that in each case there was a small cavity—approximately 1 to 2 mm in size—just above the locations at which the PPTs had been installed.

The cavities had been formed when the lag bolts were cemented into the holes in the specimen. Later, during numerical simulation of the experiments, it was determined that the presence of the cavities was the cause of the dip in the pore pressure plots. Without a cavity, the plots rise to a peak value and then subsequently decrease without a later increase. With a cavity, a dip in the pore pressure plot is encountered followed by a subsequent rise back to the previous peak pressure. The difference in the clock time at which the second peak occurred during test-1 and test-2 is attributed to the differing sizes of the cavities present in each case.

NUMERICAL SIMULATION PROCEDURES

After concluding the experimental program, the next goal in the present study was to develop a numeric simulation tool capable of predicting the pore pressure buildup in heated moist porous media. Development of such a simulation model is desirable because it can be used to perform parametric studies numerically instead of experimentally. Since numeric simulation is simpler to setup and less costly than experimental testing, it's usefulness is clear. Data predicted by the numeric models can be used either in designing further experimental studies, or as a predictive tool to be used for design and evaluation purposes.

In this study, the TOUGH code (Pruess 1987) developed by Lawrence Berkeley Laboratories at the University of California was used as the basis for the numerical modeling. TOUGH, an acronym for "transport of unsaturated groundwater and heat" is a numerical model for simulating the coupled transport of water, vapor, air and heat through porous media. It has the ability to simulate thermally driven flow and, although it was developed primarily for use in geothermal problems, the authors have successfully modified it for use in modeling moist cement mortar and concrete subjected to high temperatures.

Radiation Boundary Condition Modeling

The boundary modeling approach adopted in this work (Consolazio, McVay, Rish 1996) consists of converting the radiant boundary condition into an "effective" conductive boundary condition. In this approach, illustrated in Figure 5(b), the radiation boundary condition is represented using "effective" conductive properties. The oven (i.e. the heat source) is modeled using superelements of prescribed temperature while the specimen is modeled using "normal" size elements having the properties of cement mortar. The properties and interface distances[1] of the oven superelements are then given "effective" values. When these effective values are used within the framework of a conduction heat analysis (e.g. in TOUGH), the resulting heat fluxes are the same as would occur in a true radiant heat analysis. Thus, both the radiant boundary condition and the modeling of heat and moisture transport through the specimen can be analyzed using a conduction analysis framework.

Note that in this method of modeling the boundary condition, the oven superelements and the specimen elements are in "contact" in the sense that there are connections between them, interface areas, etc. It is across these fictitious "contact" areas that conductive heat transport occurs. The fact that these elements are in contact in the numerical model, however, in no way violates the fact that they are not connected in the actual physical (experimental) setup. The contacts are simply a construct of the numerical modeling method and nothing more.

---

[1] The interface distance is the distances between the centroid of an element and the interface between it and an adjacent element.

In creating the model, the parameters k_2 and d_2 shown in Figure 5(b) are not variables. They are the conductivity and center-to-interface distance for an element in the cement mortar model (i.e. the specimen). The conductivity k_2 is the conductivity of cement mortar and the distance d_2 is established based on the spatial discretization (i.e. "meshing") of the specimen. Thus k_2 and d_2 are fixed. However, we can choose either k_1 or d_1 arbitrarily and solve for the remaining variable to construct our "effective" boundary condition. In the present case, we choose to set d_1=d_2 and solve for the "effective" conductivity k_1 of the oven superelements.

To find the effective conductivity k_1, let us denote the conductivity of the interface between two elements as the *interface conductivity*. For two elements in contact and having different conductivities we desire to determine a value of conductivity at the interface between the elements. A particularly good choice of interpolation scheme suitable for this purpose is to make k_i the harmonic mean of k_1 and k_2 (Patankar 1980). In this case

$$k_i = \left(\frac{1-f_i}{k_1} + \frac{f_i}{k_2} \right)^{-1} \tag{1}$$

where

$$f_i = \frac{d_2}{d_1 + d_2} \tag{2}$$

Then, by equating the energy flux across the interface due to radiant heating and conductive heating (Figure 6), we can solve for an effective conductivity of the boundary superelement (Consolazio, McVay, Rish 1996). Doing so, we find that if we denote

$$h_r = \frac{\sigma\left(T_1^2 + T_2^2\right)\left(T_1 + T_2\right)}{\frac{1-\varepsilon_1}{\varepsilon_1}\frac{F_{12}}{F_{21}} + \frac{1}{F_{21}} + \frac{1-\varepsilon_2}{\varepsilon_2}} \tag{3}$$

then k_1 can be shown to be

$$k_1 = \frac{k_2 d_1 h_r}{k_2 - d_2 h_r} \tag{4}$$

which is the "effective" conductivity of the oven superelement. Note that k_1 is a function of both T_1 and T_2 since h_r is a function of T_1 and T_2. Therefore, we have an effective conductivity that is temperature dependent (as it should be for radiant heat transfer). In implementing this modeling scheme in TOUGH, the effective conductivities are updated at each iteration during the analysis, always taking into account the most current temperatures of the connected elements.

Calculation of Radiation Viewing Factors

Since radiant heat transfer occurs across space between two surfaces that are not in contact, the relative positions and orientations of the surfaces in space must be taken into account. This is accomplished by computing view factors between the surfaces and using the factors in the heat flux equations. In modeling the experimental setup of this paper, view factors corresponding to radiant heat originating from the oven surface and striking the specimen surface had to be

computed. These view factors were then used in modeling the radiation boundary condition by inserting them into Equation (3) during the TOUGH analysis.

To compute the view factors for this case, a numerical procedure was developed. The procedure consisted of discretizing the inner surface of the oven and the top surface of the specimen into a large number of elements. For efficiency, only one quarter of the specimen was modeled since it was known that the view factors would be axisymmetric over its surface. The following expressions were then derived which yield the view factor between two composite surfaces—i.e., surfaces comprised of smaller flat surface patches (see Figure 7).

$$F_{a-b} = \sum_{j=1}^{m} \left\{ \frac{\sum_{i=1}^{n} A_{a_i} F_{a_i - b_j}}{\sum_{i=1}^{n} A_{a_i}} \right\} \tag{5}$$

$$F_{a_i - b_j} = \frac{cos(\theta_i) cos(\theta_j)}{\pi r^2} A_{b_j} \tag{6}$$

In these expressions, F_{a-b} is the (total) view factor from composite surface A to composite surface B, A_{ai} is the area of the i-th patch in composite surface A, A_{bj} is the area of the j-th patch in composite surface B, and $F_{a_i - b_j}$ is the patch-to-patch view factor.

Using the expressions given above, several numerical "runs" were made using increasing levels of refinement in the surface discretization. The most refined model consisted of discretizing the oven surface with 160 patches in the vertical direction and 640 patches in the circumferential direction for a total of 102,400 patches. The surface of the specimen was discretized using a total of 300 elements (finer discretizations were also tried (for lower levels of oven discretization) but resulted in little change in the computed view factors). The resulting view factors computed using this procedure, and converted to view factors per unit area, are shown in Figure 8.

COMPARISON OF SIMULATION DATA AND EXPERIMENTAL DATA

Using the numerical simulation procedures described in the previous section, several numerical models were constructed and analyzed to try to predict the pore pressure and temperature results obtained from the experimental program. The models constructed included 1-d, 2-d, and limited 3-d models. Radiation view factors were computed as described earlier. In addition, the voids which were found to be present near the PPTs in the experimental program were modeled in some cases. Recall from earlier discussion that it was found that these voids were responsible for the "dips" in the experimental pore pressure plots.

Table 1 lists the key physical quantities that were used in the modeling. Note that the temperature of the oven was not constant throughout the simulation. It was noted during the experimental tests that the temperature in the oven dropped to approximately one-half of its initial value during the early portion of the test. This was attributed to the release of steam from surface of the specimen. The piecewise linear temperature profile used in the simulations (see Table 1) was an attempt to approximate this effect. It was found that the exact shape of the temperature

profile had little effect on the analysis results and even less effect on the peak pore pressures predicted.

Table 1. Key Physical Quantities Used in the Numerical Simulations

Cement Mortar

Density = 2100 kg/m^3
Porosity = 17.5%
Permeability = 8.324E-17 m^2
Specific heat = 921.12 J/kg C
Conductivity = 2.3 W/m C
Emmisivity = 0.88

Oven

Peak temperature = 925 C
Low temperature = ≈460 C
Emmisivity = 0.92

Oven Temperature Profile

Exp-1 Time (sec)	Exp-2 Time (sec)	Oven temperature (C)
0.0	0.0	463
100.0	100.0	740
200.0	200.0	925
550.0	450.0	925
555.0	455.0	25
1000.0	1000.0	25

2-d Simulation

In the 2-d simulation model, one-half of the specimen cross section was discretized using a variable density mesh (see Figure 9(a)). This model accounted for the following components.

- Cement mortar specimen
- Void at tip of pore pressure transducer
- Lag bolt
- Epoxy inside lag bolt

Only half of the specimen was modeled due to axisymmetry of all the components and axisymmetry of the thermal loading. Zero-flux (no flux of heat or mass) boundary conditions were used along the vertical boundaries of the model. Along the top boundary, the radiant boundary condition of the oven was modeled. The bottom boundary was modeled using very permeable superelements. Since these were superelements, the base material also acted as a heat sink. (The precise manner in which the base was modeled was found to have little effect on the results obtained due to the relatively short time frame that was of interest).

Pore pressure data and temperature data predicted by the 2-d simulation models are compared with the experimentally determined data in Figures 10 and 11. The pore pressures plotted are those occurring at a depth of approximately 19 mm from the top face of the specimen (i.e., at a position just below the void). Temperatures are plotted for the thermocouples nearest the surface (1.5 mm and 3.5 mm) and those at the level of the PPT (19 mm). One can see that there is very favorable agreement for pore pressure and favorable agreement for temperatures. Most notably, the peak pore pressures predicted by the numerical simulation very closely match the actual peak pore pressures measured experimentally.

The differences in the location of the pore pressure dips for the experimental and simulated cases are attributed to the fact that the only an approximate geometry of the void was modeled. Since the dip is a product only of the specific instrumentation setup and not a phenomenon that would normally occur in a non-instrumented specimen, the difference in the location of the dip is not of great concern. What is significant is the fact the initial peak for the experimental and simulated curves match favorably in magnitude and location (time) and that the subsequent peaks match in magnitude. Also plotted in Figure 10 is the simulation pore pressure curve for the case in which the void is omitted. It is clear from this plot that the pore pressure dip is an artifact of the void, since in this simulation no subsequent pressure rise is observed.

Good agreement between experimental and simulated temperature data is indicated by the curves in Figure 11. Transient temperatures predicted at 19 mm are seen to match quite closely with experimental data indicating proper modeling of conductive heat transfer through the specimen. At locations nearer to the surface (1.5 mm and 3.5 mm) the simulated data diverge more significantly from the experimental data. Simulation results indicated that, for points near the surface, the peak temperature reached varies considerably with change in depth. Therefore, small errors in the assumed location of the thermocouples could account, at least in part, for the difference between experimental and simulated temperatures.

3-d Simulation

The 3-d model developed to simulate the experiments consisted of a one-quarter "pie slice" (shown in Figure 9(b)). Only the inner 4mm core of the specimen was able to be modeled due to size limitations present in TOUGH[1]. The void, lag bolt, and epoxy were not modeled so that the pore pressures inside a non-instrumented specimen could be determined. In Figures 12 and 13, the pore pressure and temperature data obtained from the 3-d models are plotted through the entire depth of the specimen as time progresses. From Figure 12 one can clearly identify the interface between the fully desaturated zone and the fully saturated zones—pore pressure is seen to maximize at the boundary between these two zones. Pore pressures vary non-linearly from the peak value near the interface to atmospheric pressure at the top and bottom surfaces. As time progresses, the desaturated zone penetrates farther into the specimen. One can also clearly see the development of a very steep temperature gradient through the specimen. This suggests that not only pore pressures, but also differential thermal stresses, may play a significant role in causing spalling.

[1] The size limitations in TOUGH are related to the equation solver, not the ability to store model data. Complete 3-d models will be constructed in the near future using the newer TOUGH2 which contains conjugate gradient equation solvers appropriate for the solution of large 3-d models. Modifications for radiation boundary condition modeling and Klinkenberg's equation are currently being made to TOUGH2.

CONCLUSION

Experimental tests in which saturated cement mortar specimens were exposed to a high temperature (925C) radiant heating source have been presented. The mortar specimens were instrumented with thermocouples and pore pressure transducers so that the transient response of the specimen to thermal loading could be measured. It has been shown that very significant pore pressures—on the order of 3.1 MPa—can develop under such conditions and can be a major contributing factor to the initiation of explosive spalling.

A numerical simulation procedure has been developed and used to predict the experimental data. Radiation boundary conditions in the numerical simulation model are handled by converting radiant heat transport to "effective" conductive heat transport. Results from various simulations compare favorably with the experimentally measured data, especially with respect to predicting peak pore pressures. This suggests that the numerical modeling procedures developed herein may be used in predicting the conditions under which spalling is likely to occur. Furthermore, it means that parametric studies may be performed using numerical models to determine the effect of key material parameters (e.g., permeability, porosity, saturation level) on the buildup of pore pressure and the initiation of spalling.

Pore pressure buildup has been clearly shown to be a major factor in the occurrence of spalling but differential thermal stresses will also have an significant influence. Coupled pore pressure and differential thermal stress analyses are needed to quantify the relative importance of pore pressure buildup and thermal stress.

REFERENCES

Consolazio, G.R., McVay, M.C., Rish, J.W. III (1996), Measurement and Prediction of Pore Pressures in Saturated Cement Mortar Subjected to Radiant Heating, submitted for publication in the *ACI Materials Journal.*

Darcy, H., Les Fontaines Publiques de la Ville de Dijon, *Dalmont*, Paris, France, 1856.

Hamarthy, T.A. (1965), Effect of Moisture on the Fire Endurance of Building Elements, *ASTM Publication STP 385*, American Society of Testing and Materials.

Holman, J.P. (1990), Heat Transfer, Seventh Edition, McGraw-Hill, New York.

Jahren, P.A. (1989), Fire Resistance of High Strength/Dense Concrete With Particular Reference to the Use of Condensed Silica Fume, *ACI Publication SP 114-50, Fly Ash, Silica Fume, Slag, and Natural Pozzolans in Concrete*, American Concrete Institute.

Klinkenberg, L.J. (1941), The Permeability of Porous Media to Liquids and Gases, *American Petroleum Institute Drilling Production and Practices*, pg. 200-213.

Kodres, C.A. (1996), Moisture-Induced Pressures in Concrete Airfield Pavements, *Journal of Materials in Civil Engineering*, Vol.8, No.1, pp.41-50.

McVay, M.C., Rish, J.W. III (1995), Flow of Nitrogen and Superheated Steam Through Cement Mortar, *Journal of Thermophysics and Heat Transfer*, Vol. 9, No.4, pp. 790-792.

Patankar, Suhas V. (1980), Numerical Heat Transfer and Fluid Flow (Series in Computational Methods in Mechanics and Thermal Sciences), Taylor and Francis Publishers.

Pruess, K. (1987), TOUGH User's Guide, Earth Sciences Division, Lawrence Berkeley Laboratory, University of California, Berkeley, CA 94720, Document LBL-20700.

Sahota, M.S., Pagni, P.J. (1979), Heat and Mass Transfer in Porous Media Subject to Fires, *International Journal of Heat and Mass Transfer*, Vol. 22, pp. 1069-1081.

Sanjayan, G., Stocks, L.J. (1993), Spalling of High-Strength Silica Fume Concrete in Fire, *ACI Materials Journal*, Vol. 90, No. 2, March-April 1993, pp. 170-173.

Šelih, J., Sousa, A.C.M., Bremner, T.W. (1994), Moisture and Heat Flow in Concrete Walls Exposed to Fire, *ASCE Journal of Engineering Mechanics*, Vol. 120, No. 10, October 1994.

Smith, P. (1978), Chapter 25: Resistance to High Temperatures, in *Significance of Tests and Properties of Concrete and Concrete-Making Materials*, *Publication STP 169B*, American Society of Testing and Materials, 1978.

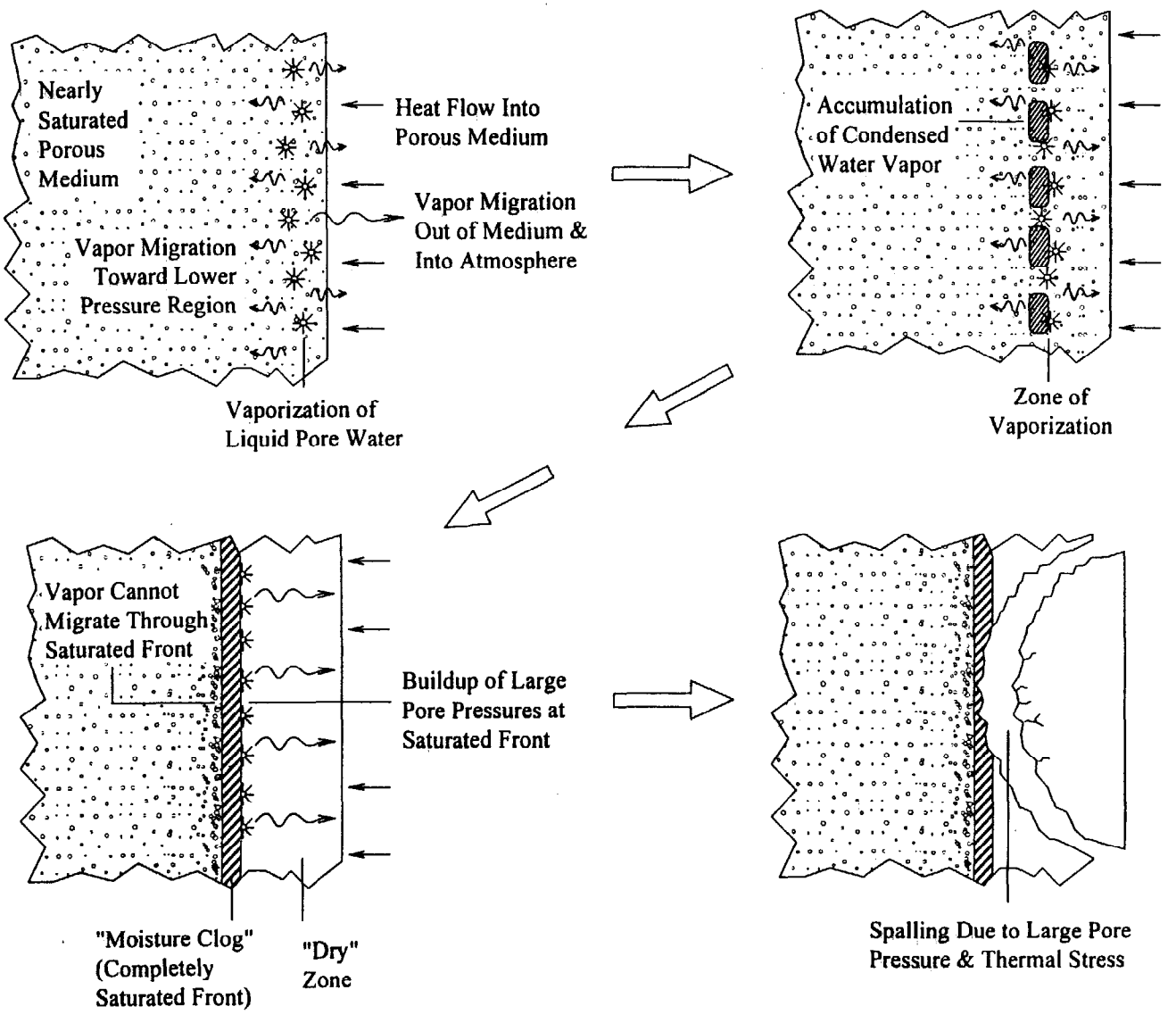

Figure 1. Sequence of Steps Leading to Fire Induced Spalling

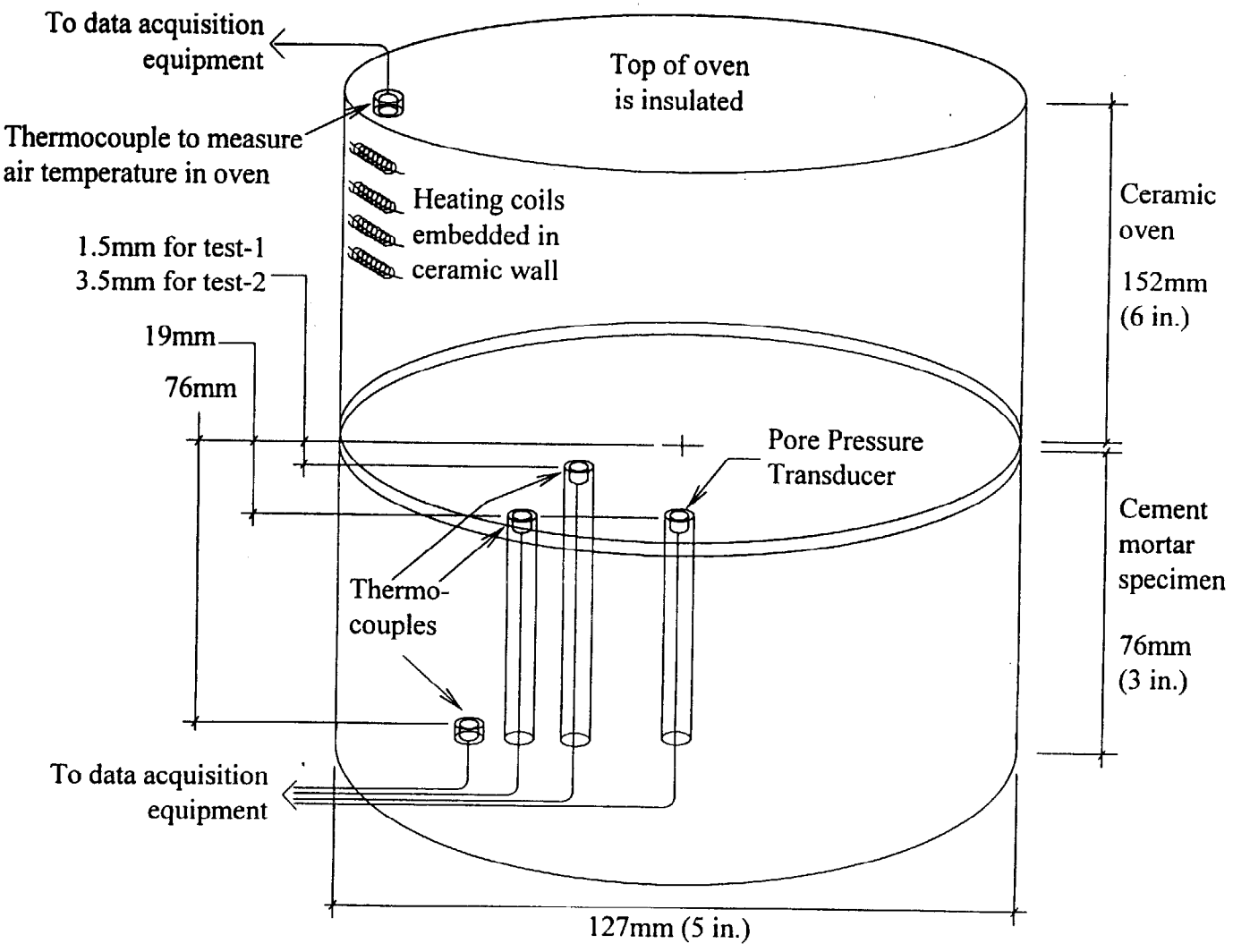

Figure 2. Instrumentation of Cement Mortar Specimen

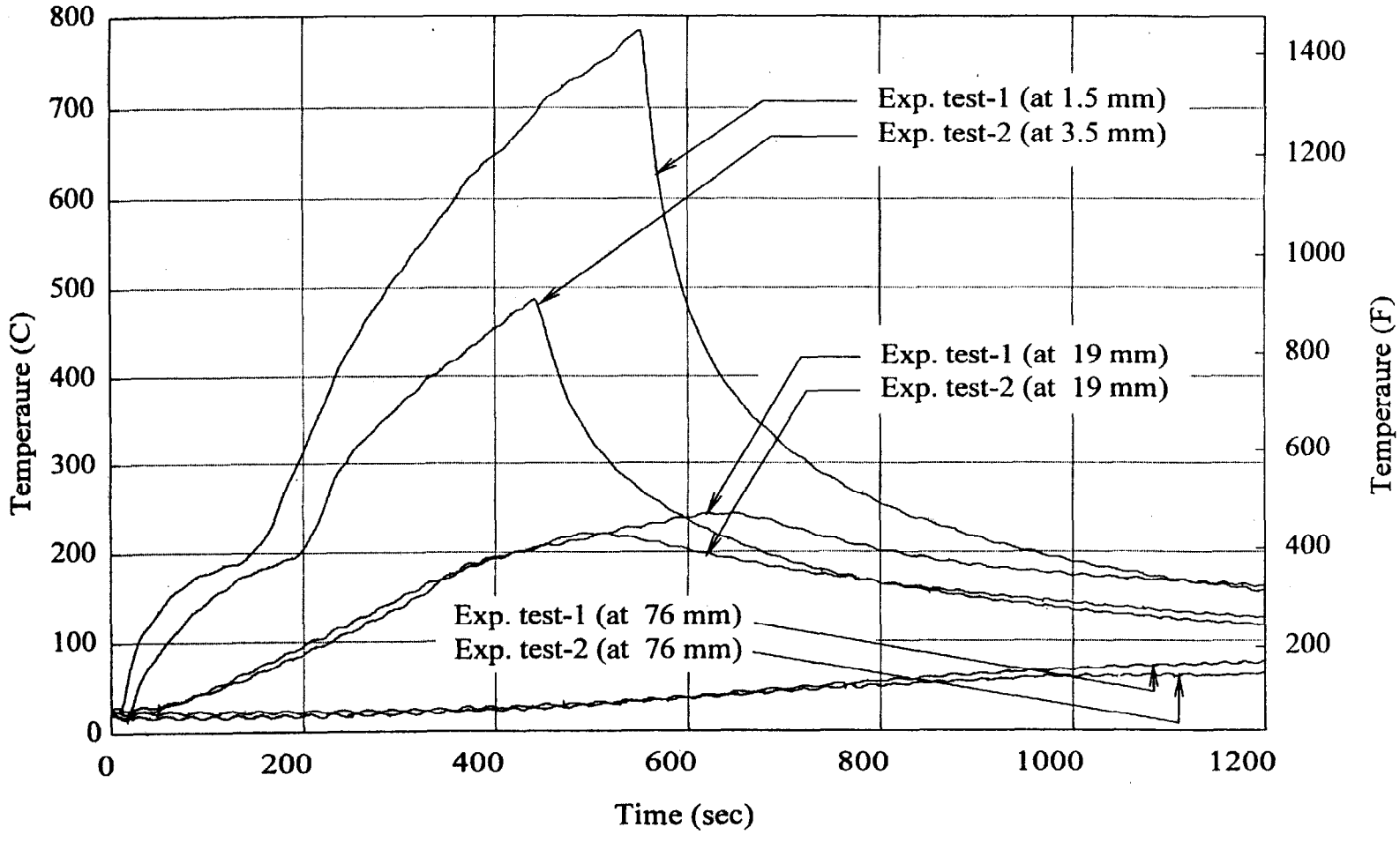

Figure 3. Transient Temperatures Due to Radiant Heating

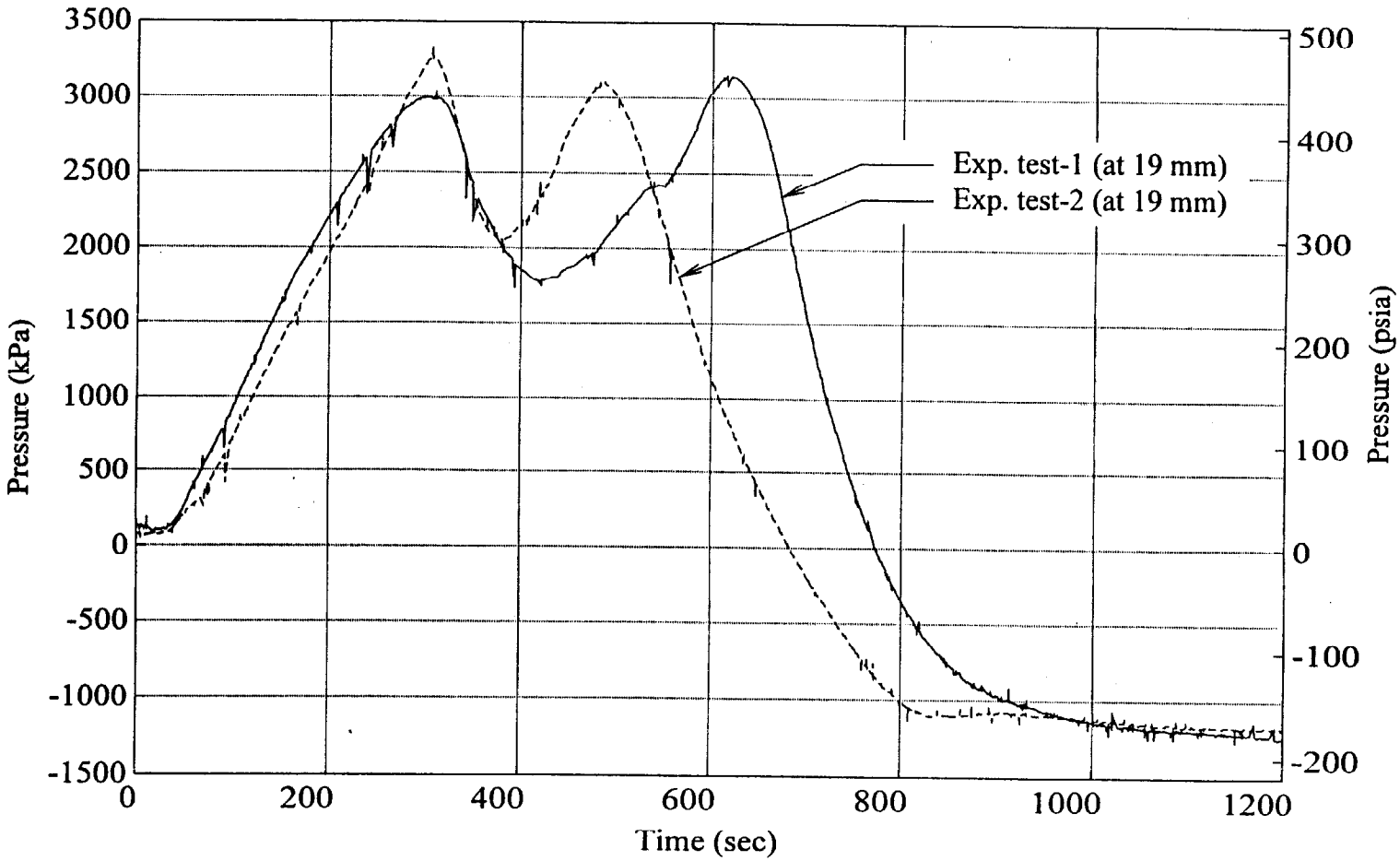

Figure 4. Transient Pore Pressures Due to Radiant Heating

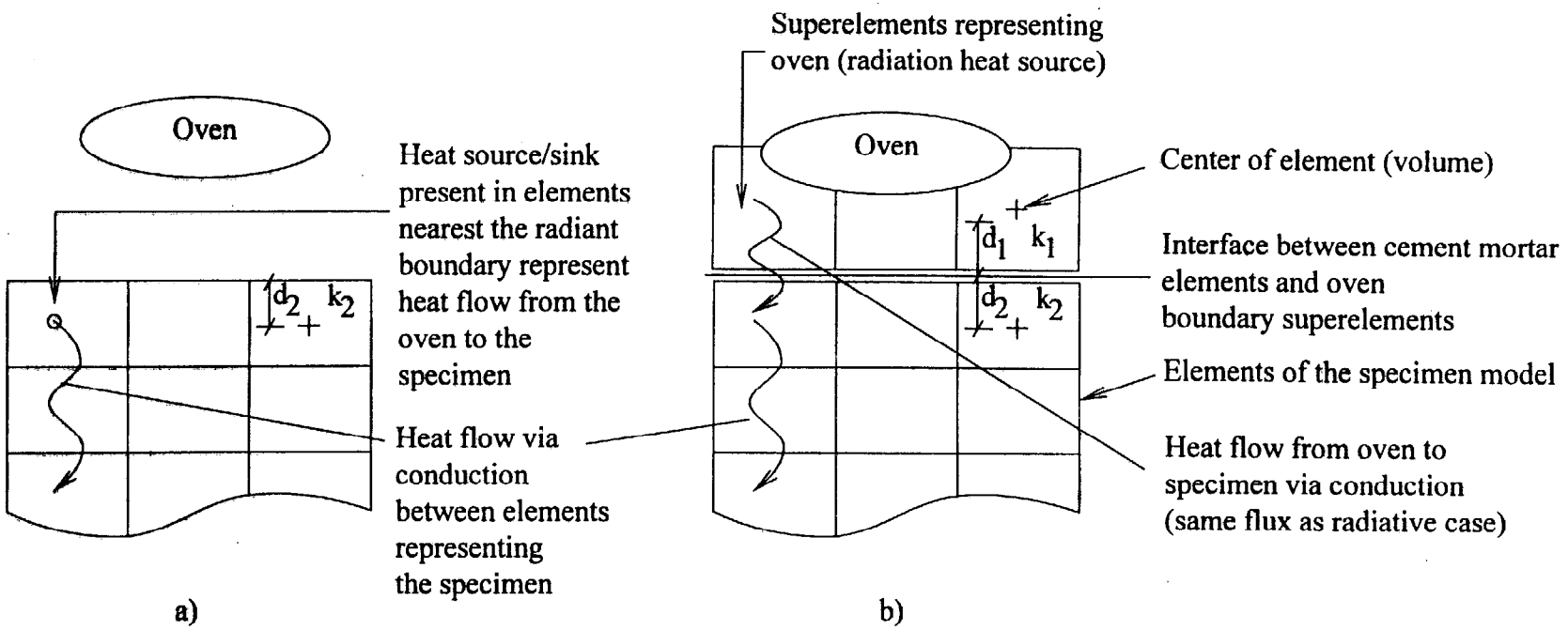

Figure 5. Modeling the Radiation Boundary Condition With a) Direct heat flux terms, and b) Effective Conduction Properties

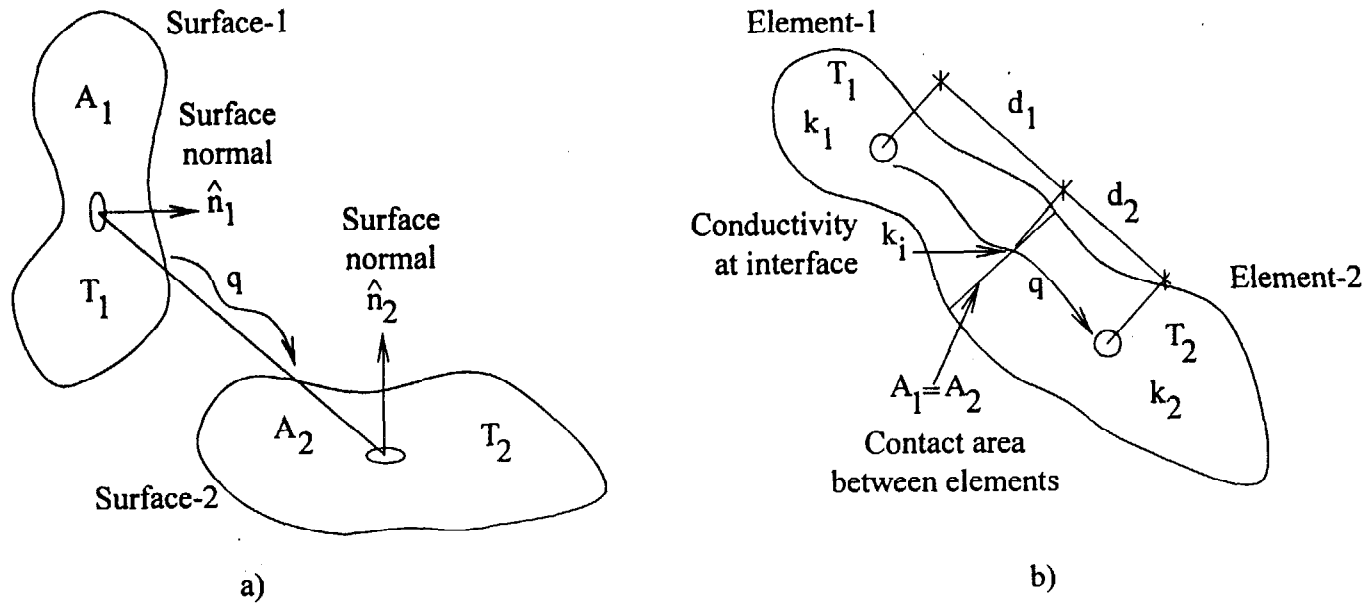

Figure 6. Heat Flux From One Body to Another
by a) Radiation and b) Conduction

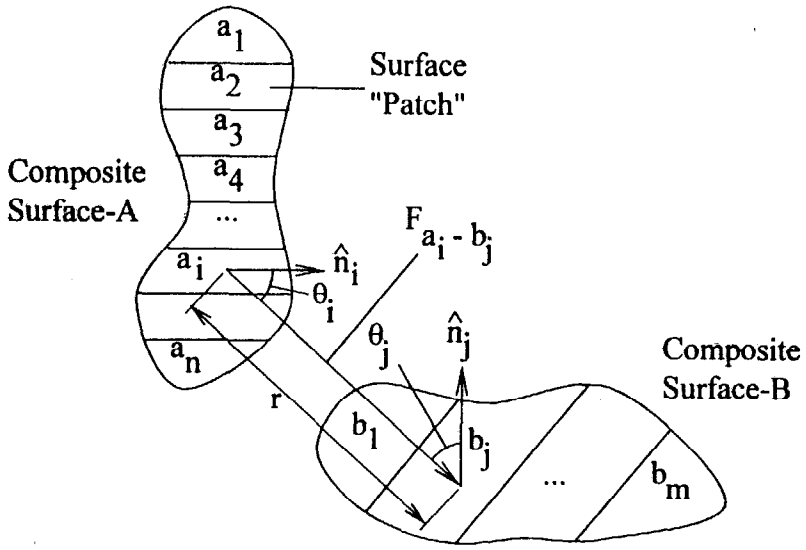

Figure 7. Computation of View Factor Between Two Composite Surfaces

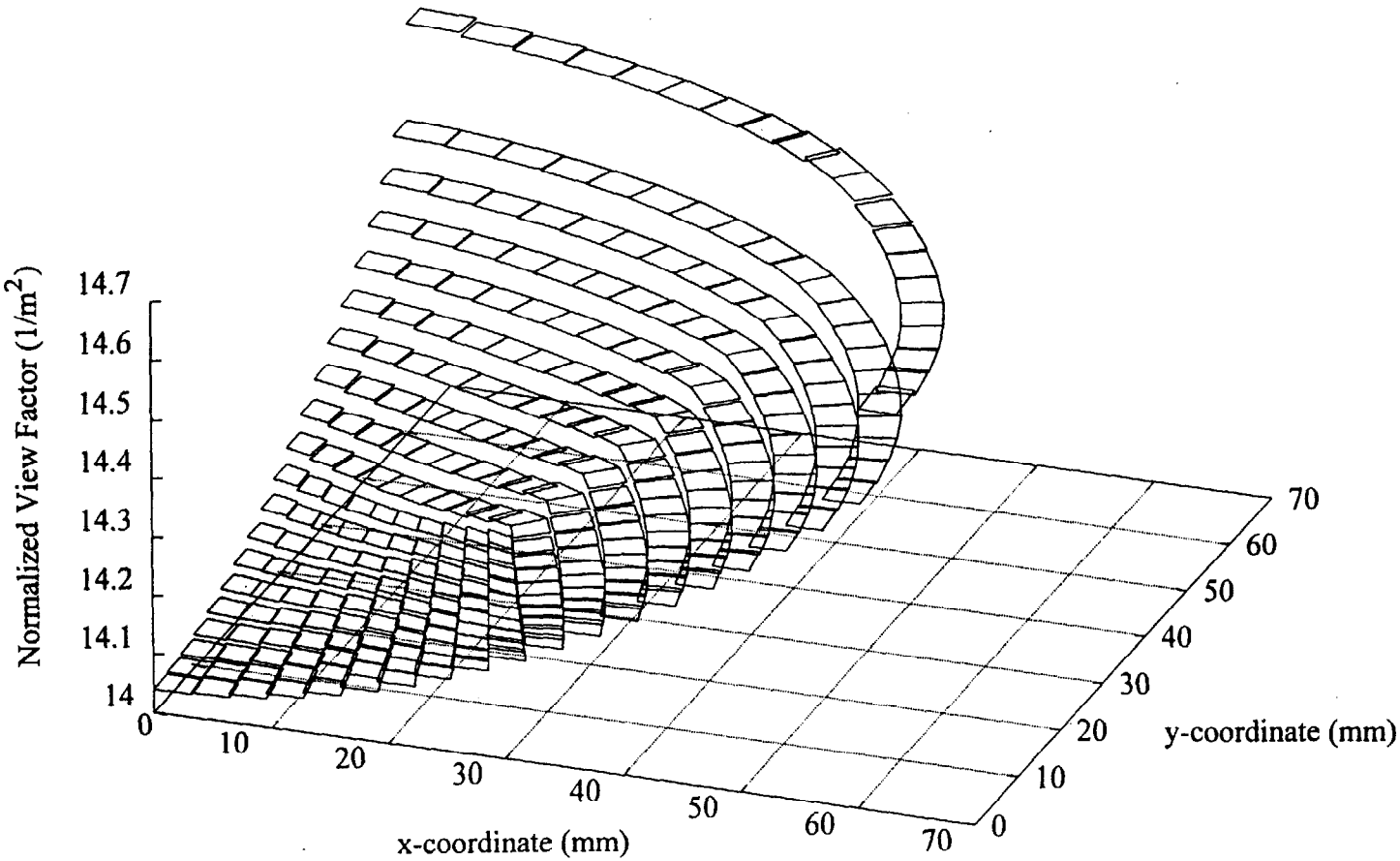

Figure 8. View Factors (Normalized Per Unit Area) Computed for Oven-Specimen Setup

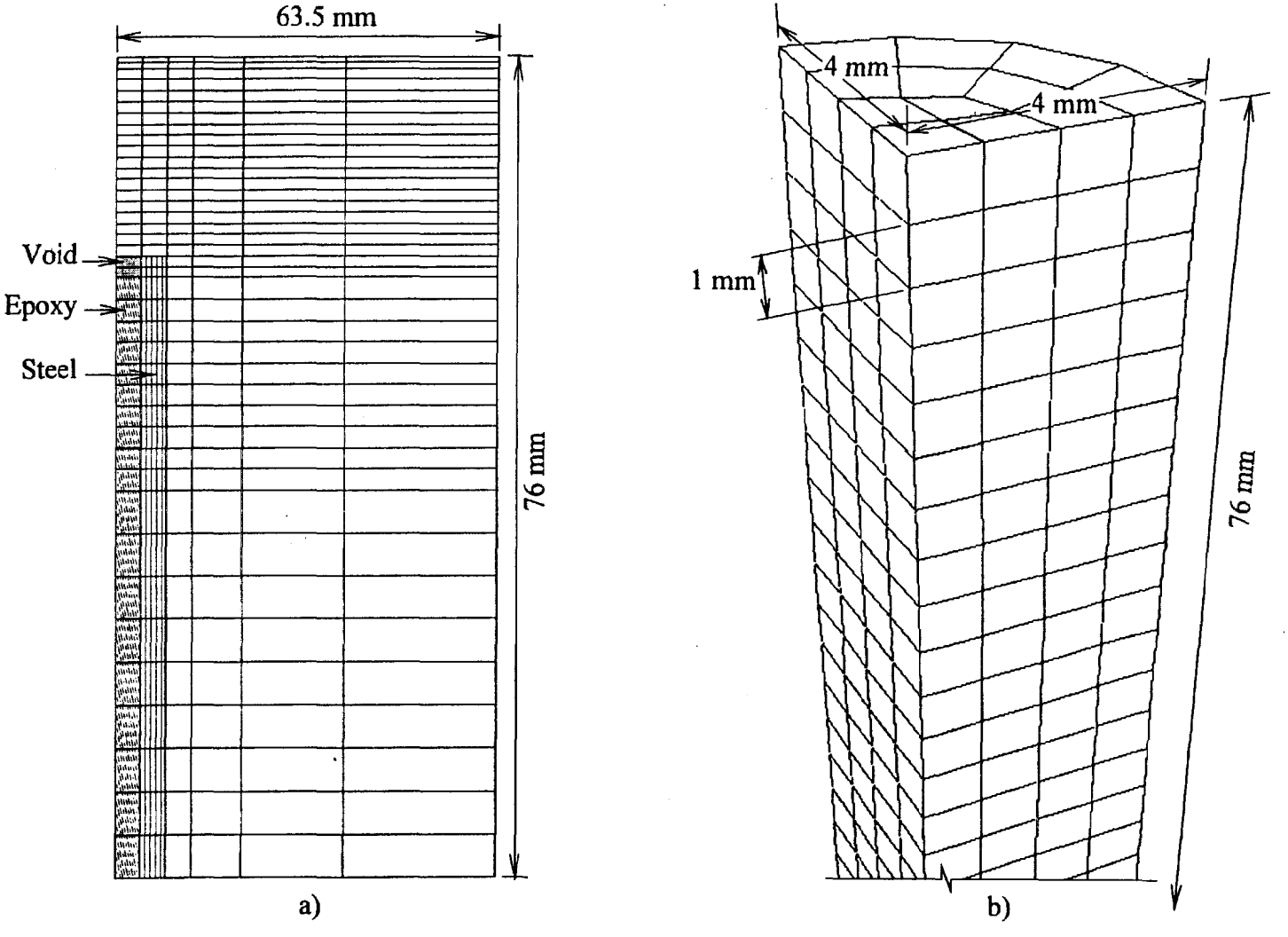

Figure 9. 2-D and Limited 3-D Simulation Models of Cement Mortar Specimen

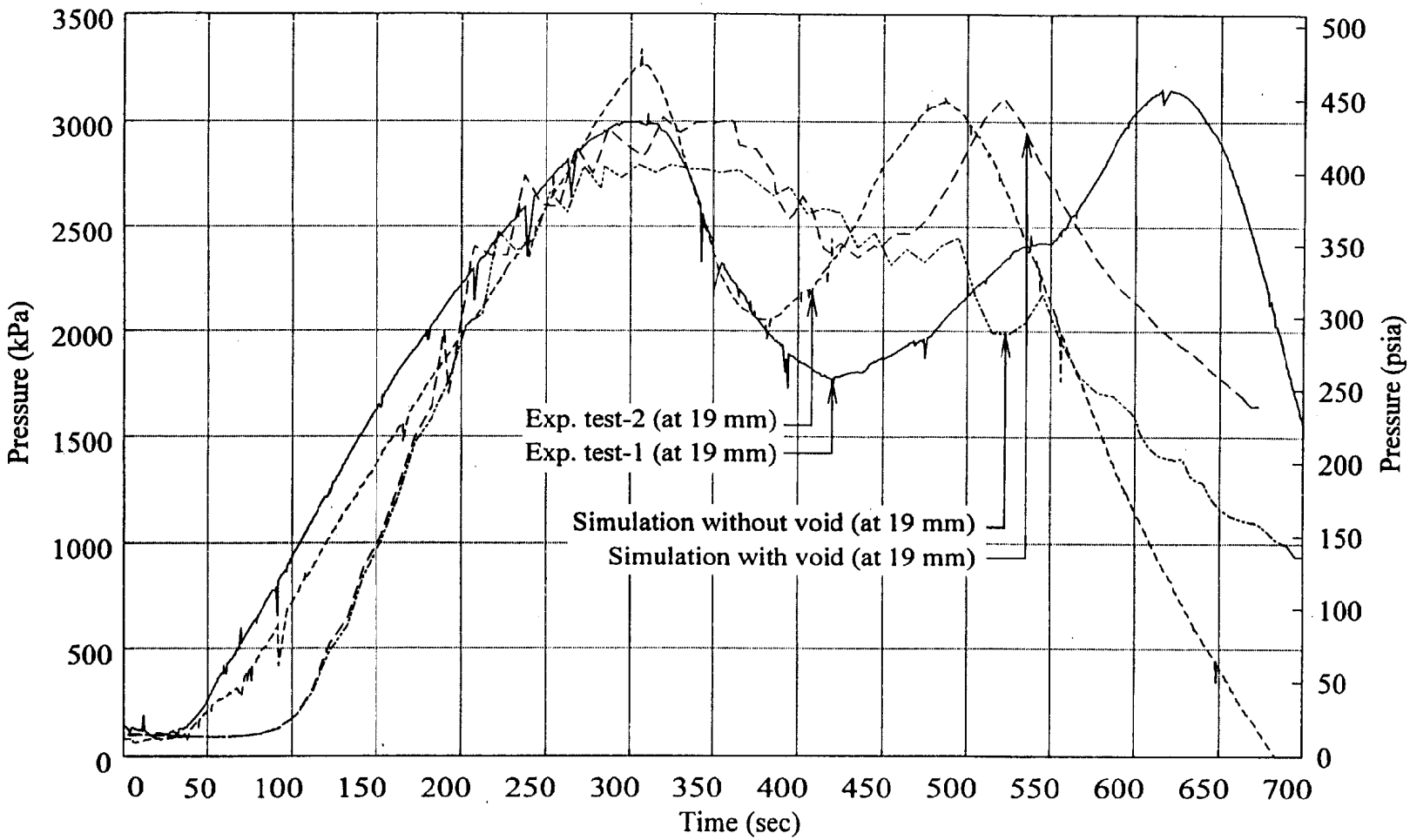

Figure 10. Pore Pressures Measured Experimentally and Predicted Using a 2-D Simulation

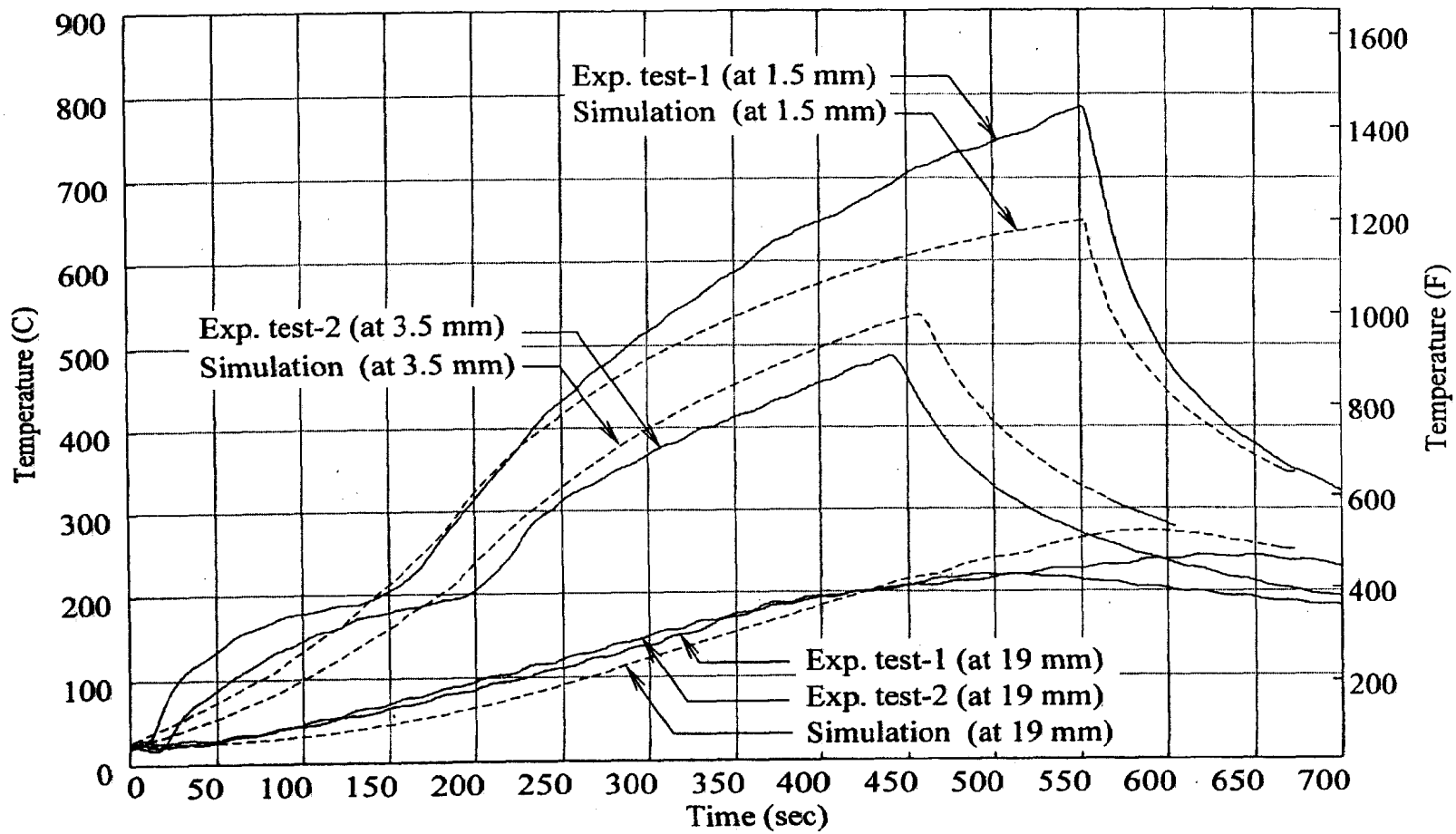

Figure 11. Temperatures Measured Experimentally and Predicted Using a 2-D Simulation Model

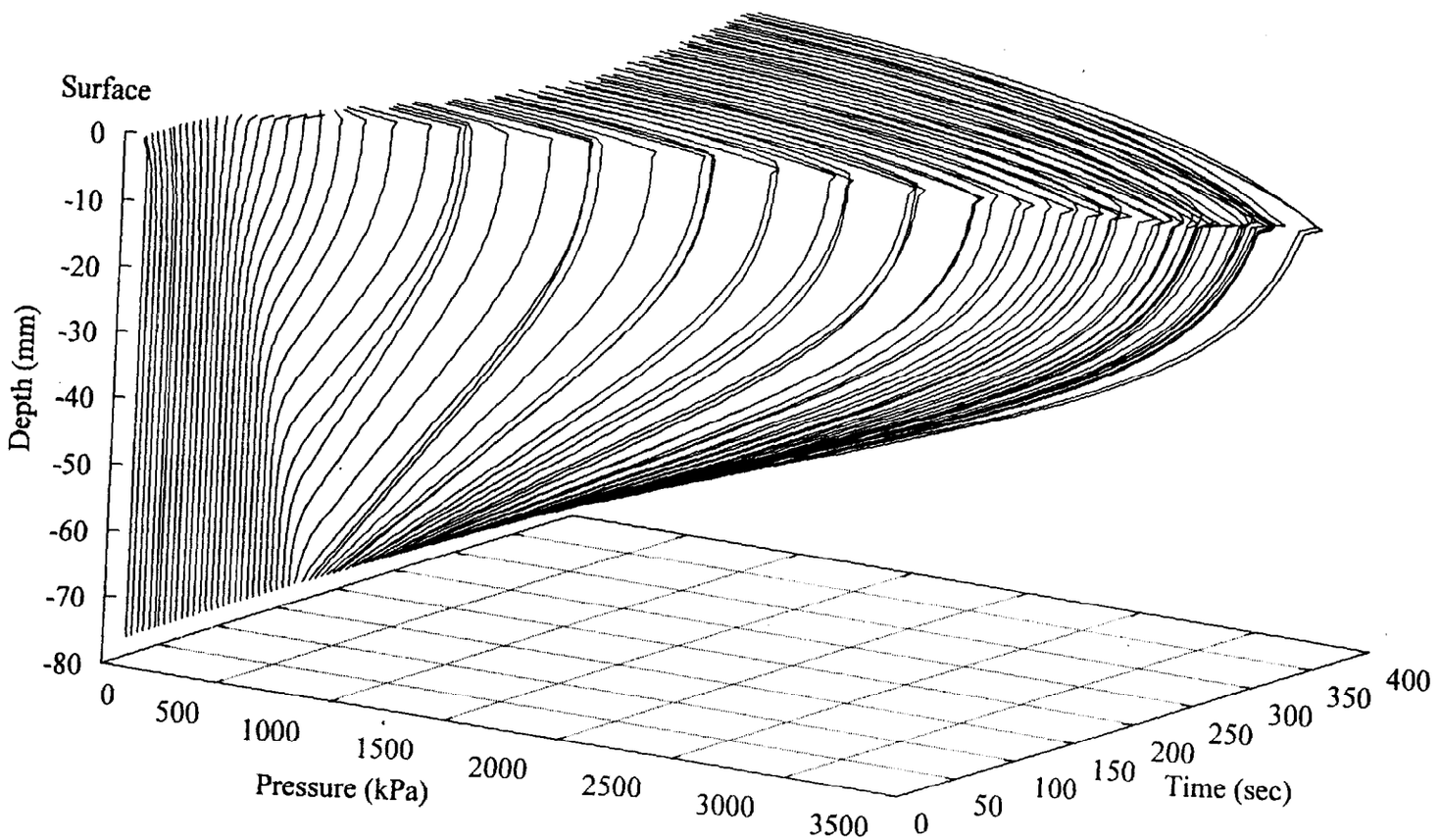

Figure 12. Variation of Pressure (as Predicted by a 3D Simulation) Through Depth of Specimen as Time Progresses

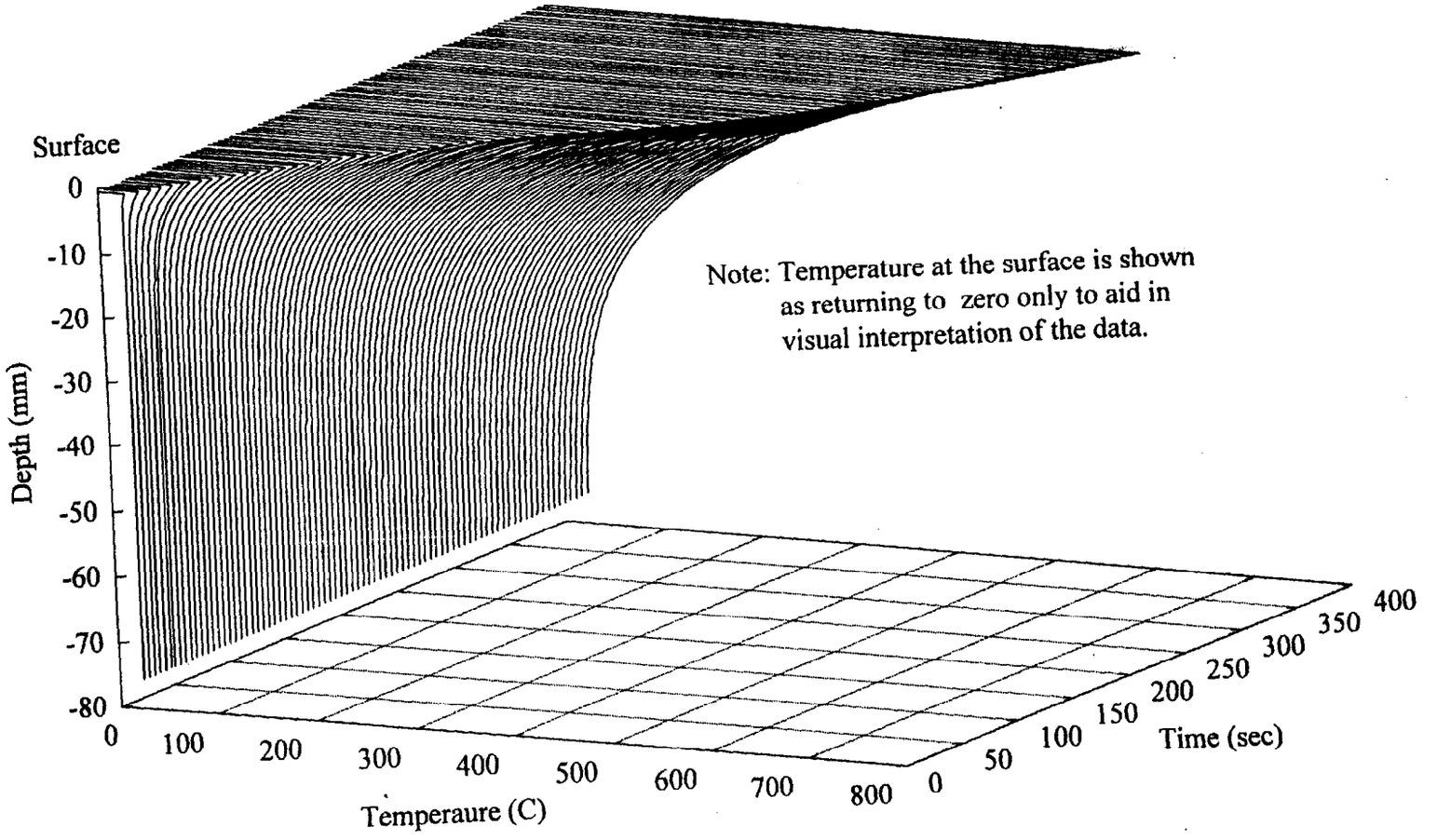

Figure 13. Variation of Temperature (as Predicted by a 3D Simulation) Through Depth of Specimen as Time Progresses